 doi:10.20944/preprints202210.0183.v1

Article

Synthesis of Carbon Black Loaded Pt Concave Nanocubes with High-Index Facets and their Enhanced Electrocatalytic Properties toward Glucose Oxidation

Xin Xu [1], Ze Ma [1], Zekun Su [1], Danqing Li [2], Xufeng Dong [1,*], Hao Huang [1,*] and Min Qi [1,]

[1] Key Laboratory of Energy Materials and Devices (Liaoning Province), School of Materials Science and Engineering, Dalian University of Technology, Dalian 116024, China; xuxin19@mail.dlut.edu.cn (X.X.); maze@mail.dlut.edu.cn (Z.M.); suzekun@mail.dlut.edu.cn (Z.S.); dongxf@dlut.edu.cn (X.D.); huanghao@dlut.edu.cn (H.H.); minqi@dlut.edu.cn (M.Q.)

[2] The Second Affiliated Hospital of Dalian Medical University, Dalian, 116023, China; lyl_lhc@163.com (D.L.)

* Correspondence: dongxf@dlut.edu.cn (X.D.); huanghao@dlut.edu.cn (H.H.); Tel.: +86-136-1085-4629 (X.D.)

Abstract: Catalyst with high catalytic activity and good stability are desirable in the electrocatalytic oxidation of glucose. Herein, Pt concave nanocubes with high-index facets (HIFs) supported by carbon black (Pt CNC/CB) are prepared through a hydrothermal method. The experimental results demonstrate that the peak current densities in different potential regions on the Pt CNC/CB anode are 0.22, 0.20, and 0.60 mA cm^{-2}, respectively. The glucose oxidation reaction shows superior performances in basic and neutral conditions than in acid conditions. Better stability is achieved by Pt CNC/CB than Pt concave nanocubes (Pt CNCs). Abundant surface defects with low-coordinated atom numbers, such as the steps, kinks, and edges, are served as active sites in the electrocatalytic oxidation of glucose. With the addition of carbon black, the catalytic activity can be improved by facilitating the full exposure of the active surface defects on the HIFs of Pt CNCs. Moreover, to address the aggregation of Pt CNCs, caused by the high surface energy of HIFs, the introduction of carbon material is an effective way to preserve the HIFs, and thus enhance the stability of the catalyst. Hence, the prepared Pt CNC/CB electrocatalyst has great potential to be applied in the electrooxidation of glucose.

Keywords: platinum; high-index facets; carbon support; glucose oxidation; electrocatalysts

1. Introduction

As the main source of energy for human metabolism, glucose is generally present in body fluids. Many favorable features, including stability, safety, and abundance, make it a good choice of fuel for implantable glucose fuel cells [1–3]. The electricity can be converted by the oxidation of glucose at the anode and the reduction of oxygen at the cathode [4–6]. This kind of glucose fuel cell is a promising power supply for various implantable medical devices, such as pacemakers, sensors, artificial heart devices, and electrodes to treat neurological diseases [7]. It is regarded as an alternative to lithium batteries, which are hard to miniaturize and restricted by a limited lifetime [8]. However, the oxidation of glucose is a difficult step, which is affected by slow kinetics [9]. To overcome this problem, the efficient catalyst for glucose oxidation has been largely studied.

Abiotic catalysts, especially noble metals are suitable candidates, which have good stability in the in vivo environment [10]. It is indicated that the electrocatalytic oxidation of glucose on platinum (Pt) single crystals is a structure-sensitive reaction [7]. The reactivity of Pt-based catalysts can be governed by varying the exposure of crystal facets, tuning the shapes, and controlling the sizes [11,12]. A large number of studies have demonstrated that nanocrystals (NCs) enclosed by high-index facets (HIFs) exhibit high catalytic properties due to the defect structures with low coordination atoms, such as steps, kinks, and edges [13–15]. So that Pt-based NCs with HIFs have been widely researched for many

Preprints (www.preprints.org) | NOT PEER-REVIEWED | Posted: 13 October 2022 doi:10.20944/preprints202210.0183.v1

catalytic applications [16–19]. However, result from the active unsaturated atoms and the high surface energy, the phenomena of atom migration and aggregation can easily occur on the surface of Pt-based NCs enclosed by HIFs, which may result in surface restructuring and the attenuation of the surface activity [20]. Hence, maintaining the high activity and preserving the HIFs of Pt-based catalyst are key issues to be addressed. A suitable material, which can provide a large surface area for Pt distribution is recommended to avoid aggregation.

So far, carbon materials as typical electrical conductivity supports have attracted extensive attention. The characteristic of the high specific surface area makes it appropriate support for different catalysts [21,22]. Generally, loading Pt-based NCs on the carbon supports (graphene, carbon nanotubes, carbon black, etc.) is an effective strategy for enhancing catalytic stability [23–27]. Zhou et al. investigated the catalytic properties of high-index faceted Pt NCs supported on carbon black (HIF-Pt/C) for ethanol electrooxidation. The HIF-Pt/C catalysts exhibit 2 ~ 3 times higher electrocatalytic activity than the commercial Pt/C catalysts for ethanol oxidation reaction, which can be attributed to their high density of atomic steps [28]. Zhao et al. prepared the 3D flowerlike Pt nanoparticle clusters onto multiwalled carbon nanotubes (MWCNTs) through the electrochemical method. The resulting Pt/MWCNTs in 3D morphology are found to exhibit significantly higher electrocatalytic activity and better stability than the dispersive morphology for glucose oxidation reaction and oxygen reduction reaction [29]. Despite numerous studies on carbon supported Pt-based catalysts with HIFs have been reported, to our knowledge, it has rarely been studied in the electrocatalytic oxidation of glucose.

In this study, Pt concave nanocubes (Pt CNCs) with HIFs supported by Vulcan XC-72R carbon black (CB) is synthesized as catalyst for the oxidation of glucose and labeled as Pt CNC/CB. The surface morphology and structure of Pt CNC/CB are characterized. The catalytic performances in glucose oxidation reaction are measured in neutral conditions. The effect of the typical Vulcan XC-72R CB support in Pt CNC/CB is evaluated. It is expected that the aggregation of Pt CNCs can be alleviated by the addition of carbon support with sufficient surface area. Therefore, the surface defect structures (steps, edges, and kinks) derived from the HIFs of Pt CNCs can be fully exposed, which are generally considered as the active sites in catalytic reactions.

2. Materials and Methods

2.1. Synthesis of Pt CNC/CB catalyst

Pt CNC/CB catalyst was synthesized by using a facile hydrothermal method (Figure 1). A specific amount of Vulcan XC-72R carbon black (CB), polyvinylpyrrolidone (PVP, MW = 28000), and glycine were added to deionized water with stirring. After that, 2 mL of H_2PtCl_6 solution (40 mM) was added to the above solution and kept stirring at room temperature for a few minutes. Then the as-prepared homogeneous solution was transferred to a Teflon-lined stainless-steel autoclave. The sealed vessel was held at 200 °C for 6 h before it cooled down to room temperature. The products were separated by centrifugation at 10000 rpm for 15 min and then purified by washing with ethanol three times.

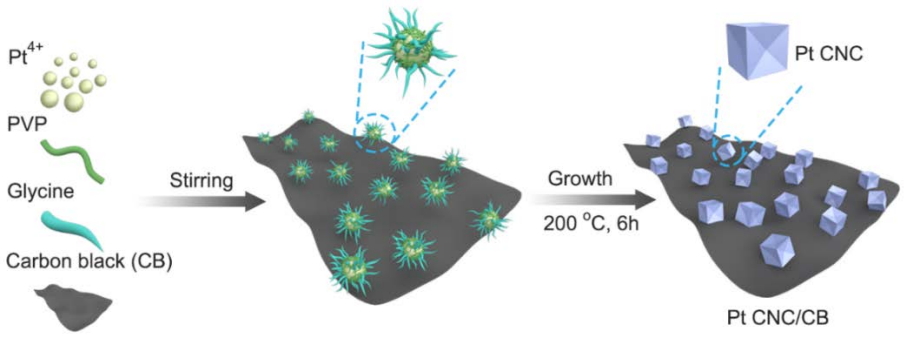

Figure 1. Schematic illustration of the synthesis of Pt CNC/CB catalyst.

 doi:10.20944/preprints202210.0183.v1

2.2. Characterization

The surface morphology of the samples was characterized by transmission electron microscopy (TEM) and high-resolution transmission electron microscopy (HRTEM) on a Tecnai G2F30 STWIN, operating at an acceleration voltage of 200 kV. X-ray photoelectron spectroscopy (XPS) measurement was conducted on a Thermo ESCALAB 250 spectrometer using a monochromic Al Kα X-ray source. The functional group information was identified by Fourier transformed infrared (FT-IR) on a Thermo Fisher 6700.

2.3. Electrochemical Measurements

Electrochemical measurements including cyclic voltammetry (CV) and chronoamperometry (CA) were performed on an M204 electrochemical workstation (Metrohm Autolab, Netherlands). The CV tests were conducted in the 0.1 M phosphate-buffered saline (PBS, pH 7.4) solution with and without the addition of 50 mM glucose. The potential range is sited from 0.079 to 1.679 V, and the scan rate is 20 mV s^{-1}. Before the electrochemical measurements, the activation of the electrode was conducted by fast CV scanning from 0.042 to 1.242 V in a 0.5 M H_2SO_4 solution. The electrochemically active surface area (ECSA) of the catalyst was calculated based on the CV curves, measured in the oxygen-free 0.5 M H_2SO_4 solution from 0.042 to 1.242 V at the scan rate of 50 mV s^{-1}. The correlations between the CV scan rate, pH value, and the current density were investigated, respectively. CA measurement was performed at the potential of 1.279 V in the 0.1 M PBS solution (pH 7.4) with the addition of 50 mM glucose. The ink for electrochemical measurements was prepared by adding the catalyst (5 mg) into ethanol (1 mL), followed by sonication for 30 min. A working electrode was prepared by loading the ink (3 μm) on a glassy carbon electrode (GCE). The saturated calomel electrode (SCE) and a Pt sheet (1 cm^2) were used as the reference and counter electrodes, respectively. All of the potentials mentioned in this article were converted to the reversible hydrogen electrode (RHE) via the equation: $E_{RHE} = E_{SCE} + 0.242 + 0.0591 \times pH$.

3. Results and Discussion

3.1. Physicochemical characterizations

Information related to surface morphology can be provided by TEM measurement. As shown in the low-resolution TEM images for Pt CNC and Pt CNC/CB samples (Figure 2a,d), uniform nanocubes are successfully synthesized in a high yield. It can be seen clearly that Pt nanocubes are uniformly dispersed on the CB support, in comparison with the pure Pt CNC sample without catalyst support. It can be illustrated that the addition of catalyst support can greatly improve the dispersibility of catalysts [28]. So that the loss of catalytic activity caused by the aggregation of active sites can be largely avoided. Sufficient exposure of the active surface is beneficial to enhance the catalytic efficiency and improve the catalytic activity of the catalyst. The average sizes of the nanocubes in Pt CNC and Pt CNC/CB are measured to be 31.06 ± 0.6 nm and 28.92 ± 0.5 nm, respectively, as determined by edge length (Figure 2c,f).

Figure 2b,e display the representative HRTEM images of Pt CNC and Pt CNC/CB samples, from which the concave structures with clear boundaries at the Pt CNC interfaces can be observed. It is well acknowledged that the angles between the facets of the projected concave nanocube and the {100} facets of an ideal cube can be used to deduce the index. Pt shows fcc crystallinity in a monometallic cluster. The selected area electron diffraction (SAED) pattern illustrates that the prepared Pt CNC is in high crystallinity along the [100] zone axis (Figure 2g). The surface Miller index is measured on an individual Pt CNC projected along [100] direction. The angles between the facets of the projected Pt CNC and the {100} facets of an ideal cube are measured to be 11°. The theoretical value of the angle between high-index planes with Miller indices (510) and the {100} planes are 11.3° [14,30]. From the comparison between the measured angles and the ideal values, it is suggested that the as-synthesized Pt CNCs are mainly enclosed by high-index (510) facets. It is reported that the high-index (510) facets can be indicated as [5(100) × (110)]

Preprints (www.preprints.org) | NOT PEER-REVIEWED | Posted: 13 October 2022 doi:10.20944/preprints202210.0183.v1

[31]. As shown in Figure 2h,i, the atomic steps on the edge of Pt CNC can be seen clearly, which is consistent with the atomic arrangement of (510) facets. Figure 2j is an atomic model of the (510) planes in Pt CNC/CB catalyst, which is established to illustrate the arrangement of atomic steps directly. Such HIFs possess a high density of step atoms, which generally constitute active sites of electrocatalysts [17].

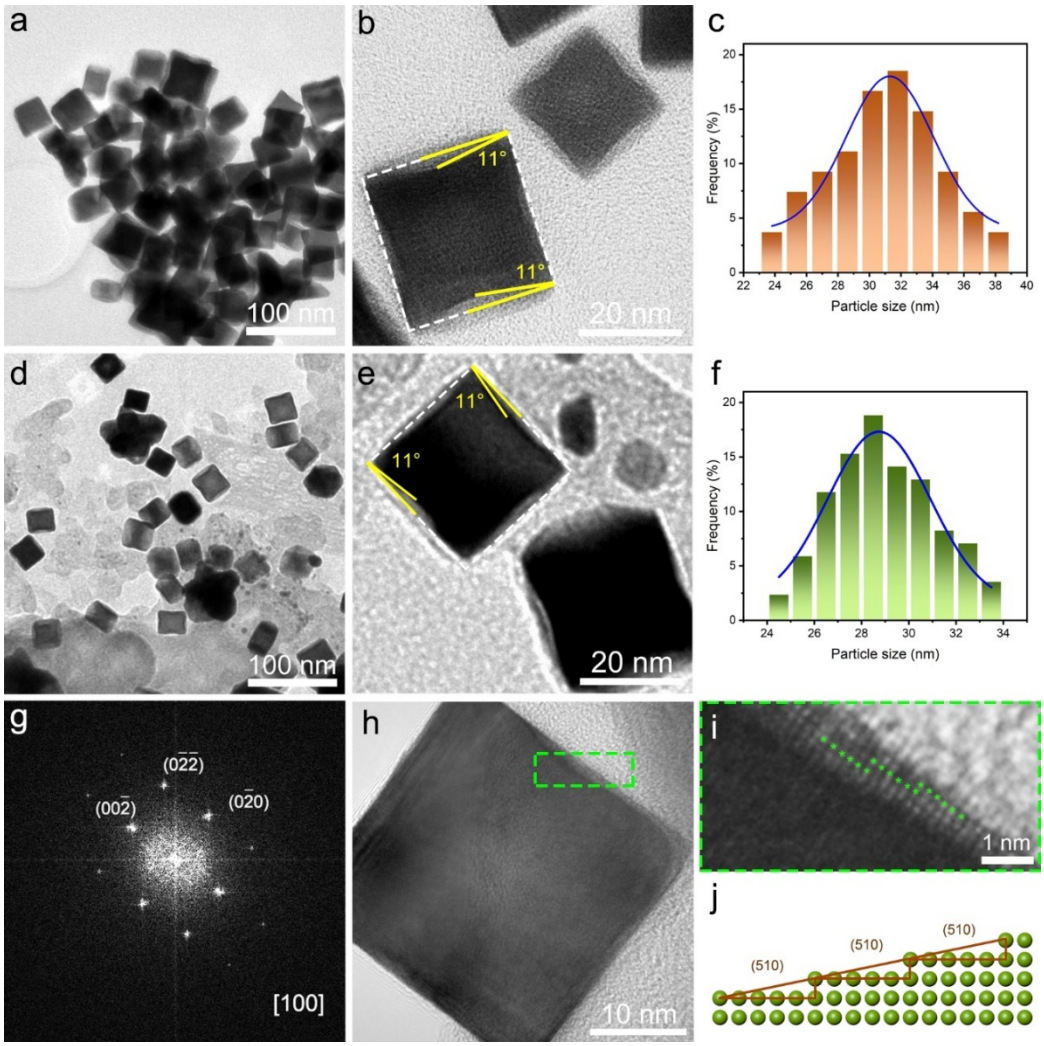

Figure 2. TEM, HRTEM images, and particle size distribution of Pt CNC (**a**, **b**, **c**), and Pt CNC/CB (**d**, **e**, **f**); SAED pattern of a single Pt CNC in Pt CNC/CB projected from the [100] direction (**g**); HRTEM images of Pt CNC/CB (**h**); magnified HRTEM image of h (**i**); atomic model of (510) planes (**j**).

XPS analysis of Pt CNC/CB is carried out to estimate the chemical state of elements. The binding energy of the C 1s (284.6 eV) is used as the standard for calibration. As shown in Figure 3a, the full survey spectrum shows major peaks for Pt 4f, C 1s, and O 1s at 71.0, 284.6, and 531.4 eV, respectively. The detection of O element is mainly originated from the air. The chemical nature of Pt 4f is further analyzed using the deconvoluted XPS spectra as shown in Figure 3b. The Pt 4f peak can be resolved into two pairs of peaks, which are identified as Pt $4f_{7/2}$ and Pt $4f_{5/2}$. The peaks located at around 71.11 and 74.44 eV represent the metallic Pt. The peaks at around 72.37 and 76.35 eV can be assigned to the Pt (Ⅱ) in PtO or $Pt(OH)_2$ species [32,33]. FT-IR spectra of Pt CNC/CB, PVP, and glycine are shown in Figure 3c. The strong characteristic peaks in PVP and glycine cannot be observed in Pt CNC/CB, which demonstrates that the redundant PVP and glycine have been removed completely after the successful synthesis of Pt CNC/CB catalyst.

Preprints (www.preprints.org) | NOT PEER-REVIEWED | Posted: 13 October 2022 doi:10.20944/preprints202210.0183.v1

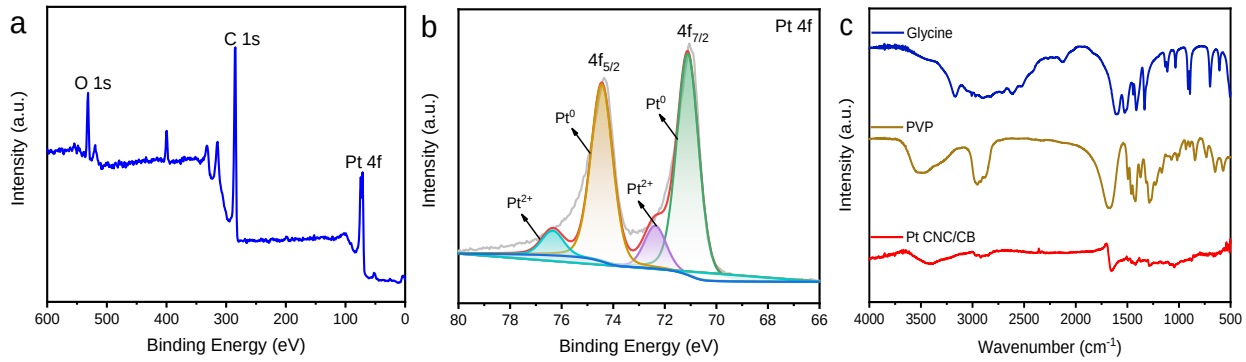

Figure 3. XPS survey spectrum of Pt CNC/CB (**a**); high-resolution XPS spectrum of Pt 4f (**b**); FT-IR spectrum of Pt CNC/CB, PVP, and glycine (**c**).

3.2. Electrochemical analysis

The ECSA of catalyst is associated with the charges in both the adsorption and desorption processes of hydrogen [34]. The ECSA value is evaluated by integrating the peak area of the CV scanning, performed in the nitrogen-saturated 0.5 M H_2SO_4 solution with a scan rate of 50 mV s^{-1}. The charge is normalized using a surface area-specific charge of an ideal one-electron transfer, which is 210 μC cm^{-2} [35,36]. As shown in Figure 4a, the peak area of Pt CNC/CB is larger than that of Pt CNC catalyst. The calculated ECSA value of Pt CNC/CB catalyst is 2.80 m^2 g^{-1}, which is approximately 2 times higher than Pt CNC (1.56 m^2 g^{-1}). The higher specific ECSA of Pt CNC/CB implies the greater dispersion of Pt CNCs, which is beneficial to the exposure of the HIFs of Pt CNCs. As for HIFs, they possess a high density of low-coordinated atoms (steps, ledges, and kinks), which can be served as highly active sites to break C–H bonds in glucose oxidation reaction.

Figure 4b shows the catalytic performance of Pt CNC/CB anode in the glucose oxidation reaction. The CV test is evaluated in the 0.1 M PBS (pH 7.4) with 50 mM glucose electrolyte. CV test in the 0.1 M PBS (pH 7.4) solution without the addition of glucose is also conducted for comparison. As shown in Figure 4b, obvious peaks can be observed from the CV curve conducted in the 0.1 M PBS (pH 7.4) with 50 mM glucose electrolyte, which demonstrates the oxidation reaction of glucose. During the oxidation process, the glucose is first electrooxidized to gluconolactone and then hydrolyzed to gluconic acid [37,38]. The electrocatalytic oxidation of glucose can be characterized by the peaks at three potential ranges. The oxidation peak in the hydrogen region (0.15 ~ 0.35 V) demonstrates the adsorption of glucose molecules on the surface of Pt CNC/CB anode. The bond breaking between the hemiacetal carbon and the attached hydrogen atom is considered as the rate-limiting step in glucose electrooxidation reaction [9,39,40]. In this step, both the glucose molecule and the hydrogen atom are adsorbed on the electrode surface through the Pt CNC/CB catalyst (Equations 1–3).

$$Pt + C_6H_{12}O_6 \rightarrow Pt(C_6H_{11}O_6)_{ads} + H \quad (1)$$

$$Pt + H \rightarrow Pt - H \quad (2)$$

$$Pt - H \rightarrow Pt + H^+ + e^- \quad (3)$$

In the double-layer region (0.4 ~ 1.0 V), as the applied potential increases, abundant of OH_{ads} species are formed through the fast decomposition of water. According to the 'Incipient Hydrous Oxide Adatom Mediator' model (IHOAM) proposed by Burke, the incipient hydrous oxide layer of OH_{ads} is generated through a premonolayer oxidation step on the surface of active metals, which can mediate the oxidation of glucose [41,42]. The active OH_{ads} layer is more likely to generate on the active sites with low lattice coordination values and disconnected areas such as the edges. Thus, the concave structure in the Pt CNC/CB catalyst is considered as a favorable structure which can serve as active site for electrocatalytic oxidation of glucose (Equations 4–6).

Preprints (www.preprints.org) | NOT PEER-REVIEWED | Posted: 13 October 2022 doi:10.20944/preprints202210.0183.v1

$$H_2O \rightarrow OH_{ads} + H^+ + e^- \quad (4)$$

$$C_6H_{11}O_6 + (OH)_{ads} \rightarrow C_6H_{10}O_6 + H_2O \quad (5)$$

$$C_6H_{10}O_6 + H_2O \rightarrow C_6H_{12}O_7 \quad (6)$$

A peak located at the potential over 1.1 V can be observed, which is regarded as the oxygen region. In this region, the active OH_{ads} species on the surface of Pt CNC/CB are stripped and replaced by the O_{ads} species, which exhibit less activity than OH_{ads}. The O_{ads} adsorbed on the surface of the Pt CNC/CB catalyst facilitate the formation of the PtO layer, which can oxidize the glucose molecule directly (Equations 7–8) [38]. The peak current densities measured on the Pt CNC/CB anode are 0.22, 0.20, and 0.60 mA cm^{-2}, respectively. It exhibits higher catalytic activity than Pt CNC and commercial Pt/C catalysts, compared with our previous study [43]. The improved catalytic activity can be attributed to the addition of CB catalyst support, which largely improves the dispersity of the Pt CNCs and lets the active HIFs of Pt CNCs exposed adequately.

$$C_6H_{12}O_6 + PtO \rightarrow C_6H_{10}O_6 + Pt + H_2O \quad (7)$$

$$C_6H_{10}O_6 + H_2O \rightarrow C_6H_{12}O_7 \quad (8)$$

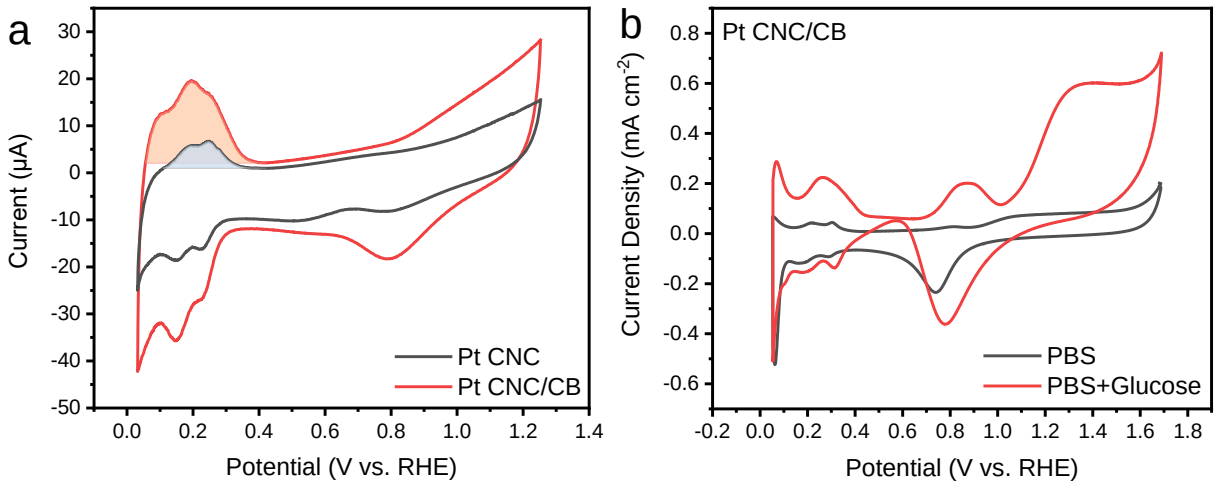

Figure 4. CV curves of Pt CNC/CB and Pt CNC in a 0.5 M H_2SO_4 solution (**a**); CV curves of Pt CNC/CB in the 0.1 M PBS (pH 7.4) solution with and without 50 mM glucose (**b**).

As shown in Figure 5a, a series of CV curves of the fabricated Pt CNC/CB anode are measured by varying the scan rate from 10 mV s^{-1} to 200 mV s^{-1} in a mixing solution of 0.1 M PBS (pH 7.4) and 50 mM glucose. It can be detected from the CV curves that as the scan rate increases, the peak current densities present an upward trend. Figure 5b shows the linear relationship between the current density of the oxidation peak and the square root of the scan rate, which reveals the typical diffusion-controlled electrochemical behavior on the Pt CNC/CB anode [44].

Catalytic performance of Pt CNC/CB electrode toward glucose oxidation in the mixing solution of 0.1 M PBS and glucose are detected at different pH. The pH values of 6, 7, and 10 are selected on behalf of the acidic, neutral, and basic conditions. From Figure 5c, the CV curve detected in the solution of pH 6 exhibits the highest peak current density than at other pH values in the hydrogen region, which can be associated with the adequate hydrogen ions in the acidic electrolyte. However, in the double-layer region, the peak of current density in the basic conditions is much more obvious than those in the acidic and neutral solutions. In the basic environment, abundant of OH^- are likely to be adsorbed on the surface of Pt CNC/CB electrode, which can be served as active sites for the glucose oxidation reaction. With the increase of the applied potential, the active OH_{ads} are replaced by O_{ads} in the oxygen region. The peaks observed in the basic and neutral electrolyte in the oxygen region is higher than that in the acidic conditions. Thus, the reactivity of the

Preprints (www.preprints.org) | NOT PEER-REVIEWED | Posted: 13 October 2022 doi:10.20944/preprints202210.0183.v1

electrocatalytic oxidation of glucose in the electrolyte shows a sequence as basic > neutral > acidic [42].

The stability of Pt CNC/CB and Pt CNC electrodes in glucose oxidation reaction are further evaluated by CA tests at 1.279 V for 60 s. As shown in Figure 5d, the CA curves demonstrate a fast decrease initially and then become stable. After 60 s, the steady current densities of glucose oxidation on Pt CNC/CB and Pt CNC electrodes are 0.061 mA cm^{-2} and 0.0062 mA cm^{-2}, respectively. It reveals that the Pt CNC/CB electrode exhibits higher activity and stability compared to the Pt CNC electrode. It may be benefit from the loading of Pt CNCs on the CB catalyst support, which effectively facilitates the exposure of the active HIFs of Pt CNCs.

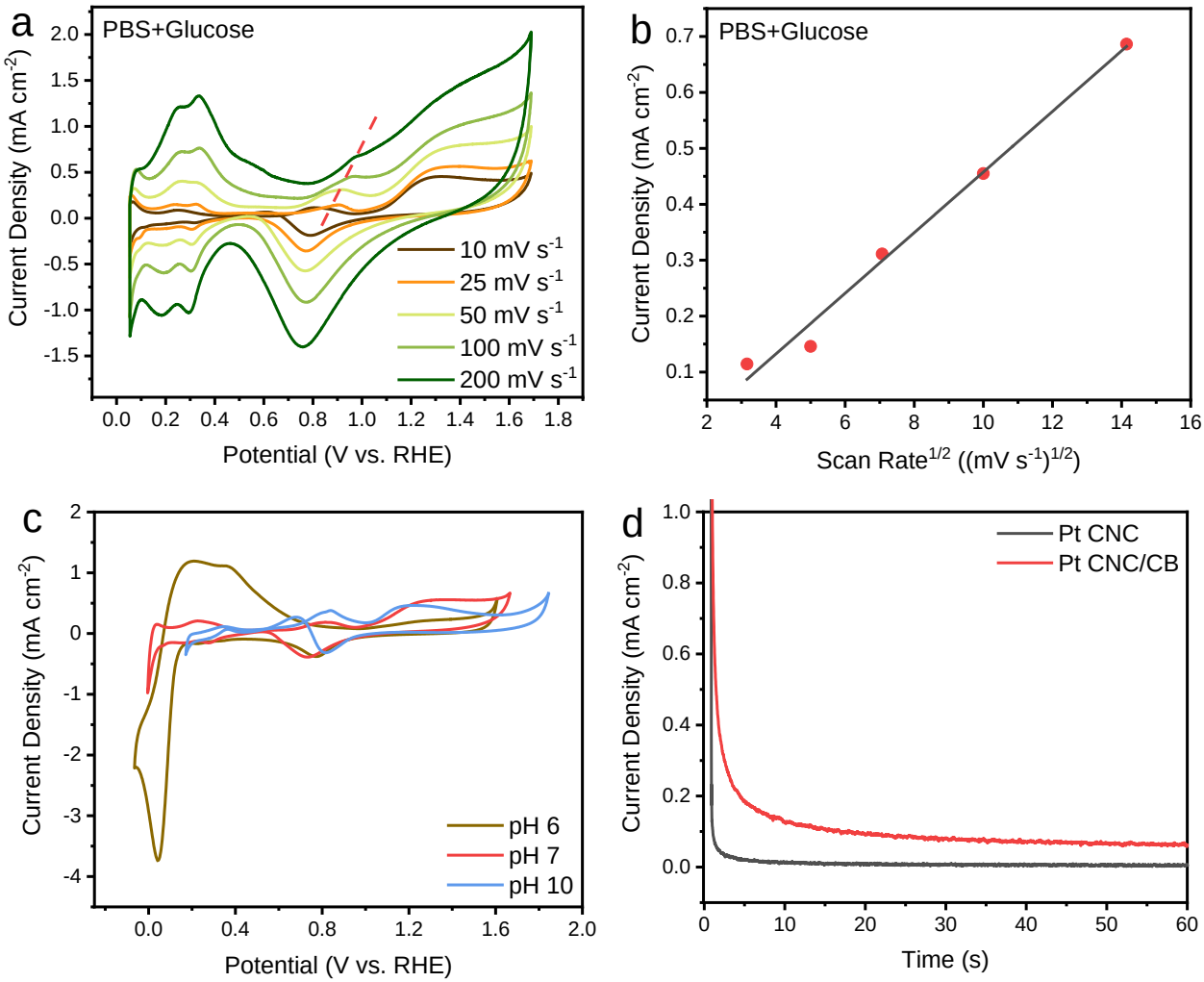

Figure 5. CV curves of Pt CNC/CB in the 0.1 M PBS (pH 7.4) and 50 mM glucose electrolyte at different scan rates (v = 10, 25, 50, 100 and 200 mV s^{-1}) (**a**); scan rate dependence of the current density for Pt CNC/CB in the 0.1 M PBS (pH 7.4) solution with 50 mM glucose (**b**); CV curves of Pt CNC/CB in the 0.1 M PBS solution with 50 mM glucose at different pH (pH = 6, 7, and 10) (**c**); CA curves of Pt CNC/CB electrode at 1.279 V in the 0.1 M PBS (pH 7.4) and 50 mM glucose electrolyte (**d**).

Compared with the conventional Pt nanoparticle catalysts, the catalytic activity of Pt CNC is greatly improved by a high density of atomic steps, edges, and kinks provided by the HIFs on the surface of Pt CNCs, which are served as active sites in the glucose oxidation reaction. During the catalytic process, the discontinuous structures with low coordination numbers are more likely to adsorb or bond with the glucose, OH_{ads}, O_{ads}, and the intermediates. The addition of the CB catalyst support effectively increases the dispersion of Pt CNCs, which facilitates the full exposure of the active structures. Sufficient exposure of active sites benefits to improve the catalytic efficiency, and thus enhance the catalytic activity of Pt CNC/CB. Moreover, the stability of Pt CNC/CB is strengthened by

 doi:10.20944/preprints202210.0183.v1

decorating the Pt CNCs on the CB catalyst support with a large surface area, which can effectively avoid the agglomeration of the Pt CNCs.

4. Conclusions

In summary, Pt CNC/CB catalyst is synthesized via a facile hydrothermal method. The prepared catalyst represents high catalytic activity and good stability for the electrocatalytic oxidation of glucose in the neutral conditions. Reasons for the enhanced catalytic properties can be expressed as follows. Firstly, the CB catalyst support provides a large surface area for the sufficient dispersion of Pt CNCs, which facilitates the full exposure of the active HIFs. Secondly, the good chemical stability and remarkable mechanical properties of carbon material help to improve the stability of Pt CNC/CB catalyst. Thirdly, high densities of atomic steps, edges, and kinks derived from the HIFs of Pt CNC are favorable for boosting the electrocatalytic activity of Pt CNC/CB catalyst. This work provides an alternative catalyst for further application in implantable glucose fuel cells and electrochemical biosensors, which are capable for the power supply and glucose detection in the human body.

Author Contributions: Conceptualization, data curation, X.X. and Z.M.; methodology, X.X., Z.M., D.L. and H.H.; software, X.X., Z.M. and Z.S.; validation, D.L., X.D., H.H. and M.Q.; formal analysis, Z.S.; investigation, Z.M.; writing—original draft preparation, visualization, project administration, X.X.; writing—review and editing, X.X. and X.D.; resources, supervision, funding acquisition, X.D. and M.Q. All authors have read and agreed to the published version of the manuscript.

Funding: This research was funded by the Fundamental Research Funds for the Central Universities of China, grant number DUT22YG201.

Data Availability Statement: The data presented in this study are available on request from the corresponding author.

Acknowledgments: We acknowledged the support from the Fundamental Research Funds for the Central Universities of China.

Conflicts of Interest: The authors declare no conflict of interest.

References

1. Cosnier, S.; Le Goff, A.; Holzinger, M. Towards glucose biofuel cells implanted in human body for powering artificial organs: Review. *Electrochem. Commun.* **2014,** *38*, 19–23.
2. Bahari, M.; Malmberg, M. A.; Brown, D. M.; Nazari, S. H.; Lewis, R. S.; Watt, G. D.; Harb, J. N. Oxidation efficiency of glucose using viologen mediators for glucose fuel cell applications with non-precious anodes. *Appl. Energy* **2020,** *261*, 114382.
3. Li, Q.; Shao, Z.; Han, T.; Zheng, M.; Pang, H. A high-efficiency electrocatalyst for oxidizing glucose: Ultrathin nanosheet Co-based organic framework assemblies. *ACS Sustainable Chem. Eng.* **2019,** *7*, 8986–8992.
4. Yao, S. J.; Appleby, A. J.; Geisel, A.; Cash, H. R.; Wolfson, S. K. Anodic oxidation of carbohydrates and their derivatives in neutral saline solution. *Nature* **1969,** *224*, 921–922.
5. Santiago, Ó.; Navarro, E.; Raso, M. A.; Leo, T. J. Review of implantable and external abiotically catalysed glucose fuel cells and the differences between their membranes and catalysts. *Appl. Energy* **2016,** *179*, 497–522.
6. Siva, G.; Aziz, M. A.; Gnana Kumar, G. Engineered tubular nanocomposite electrocatalysts based on cus for high-performance, durable glucose fuel cells and their stack. *ACS Sustainable Chem. Eng.* **2018,** *6*, 5929–5939.
7. Mello, G. A. B.; Cheuquepán, W.; Feliu, J. M. Investigation of reactivity of Pt basal planes towards glucose electro-oxidation in neutral solution (pH 7): Structure-sensitivity dependence and mechanistic study. *J. Electroanal. Chem.* **2020,** *878*, 114549.
8. Gonzalez-Solino, C.; Bernalte, E.; Metcalfe, B.; Moschou, D.; Di Lorenzo, M. Power generation and autonomous glucose detection with an integrated array of abiotic fuel cells on a printed circuit board. *J. Power Sources* **2020,** *472*, 228530.
9. Huang, J.; Simons, P.; Sunada, Y.; Rupp, J. L. M.; Yagi, S. Pt-catalyzed D-glucose oxidation reactions for glucose fuel cells. *J. Electrochem. Soc.* **2021,** *168*, 64511.
10. Kerzenmacher, S.; Ducrée, J.; Zengerle, R.; von Stetten, F. Energy harvesting by implantable abiotically catalyzed glucose fuel cells. *J. Power Sources* **2008,** *182*, 1–17.
11. Leong, G. J.; Schulze, M. C.; Strand, M. B.; Maloney, D.; Frisco, S. L.; Dinh, H. N.; Pivovar, B.; Richards, R. M. Shape-directed platinum nanoparticle synthesis: Nanoscale design of novel catalysts. *Appl. Organomet. Chem.* **2014,** *28*, 1–17.
12. Duan, S.; Du, Z.; Fan, H.; Wang, R. Nanostructure optimization of platinum-based nanomaterials for catalytic applications. *Nanomaterials* **2018,** *8*, 949.

13. Poerwoprajitno, A. R.; Gloag, L.; Cheong, S.; Gooding, J. J.; Tilley, R. D. Synthesis of low- and high-index faceted metal (Pt, Pd, Ru, Ir, Rh) nanoparticles for improved activity and stability in electrocatalysis. *Nanoscale* **2019,** *11*, 18995–19011.
14. Yu, T.; Kim, D. Y.; Zhang, H.; Xia, Y. Platinum concave nanocubes with high-index facets and their enhanced activity for oxygen reduction reaction. *Angew. Chem. Int. Ed.* **2011,** *50*, 2773–2777.
15. Jeyaraj, M.; Gurunathan, S.; Qasim, M.; Kang, M.-H.; Kim, J.-H. A comprehensive review on the synthesis, characterization, and biomedical application of platinum nanoparticles. *Nanomaterials* **2019,** *9*, 1719.
16. de Andrade, R. N.; Perini, N.; Vieira, J. L.; Gallo, J. M. R.; Sitta, E. Glycerol electrooxidation catalyzed by Pt-Sb supported in periodic mesoporous carbon CMK-3 and CMK-5. *J. Electroanal. Chem.* **2021,** *896*, 115158.
17. Wei, L.; Liu, F.; Jiang, X.; Yang, Y.-H.; Sheng, T.; Xu, Q.-Q.; Zhao, X.-S.; Fan, Y.-J. High-index faceted Pt-Ru alloy concave nanocubes with enhancing ethanol and CO electro-oxidation. *Electrochim. Acta* **2021,** *396*, 139266.
18. Shen, M.; Xie, M.; Slack, J.; Waldrop, K.; Chen, Z.; Lyu, Z.; Cao, S.; Zhao, M.; Chi, M.; Pintauro, P. N.; Cao, R.; Xia, Y. Pt–Co truncated octahedral nanocrystals: A class of highly active and durable catalysts toward oxygen reduction. *Nanoscale* **2020,** *12*, 11718–11727.
19. Lai, J.; Niu, W.; Li, S.; Wu, F.; Luque, R.; Xu, G. Concave and duck web-like platinum nanopentagons with enhanced electrocatalytic properties for formic acid oxidation. *J. Mater. Chem. A* **2016,** *4*, 807–812.
20. Wang, Y.; Zhuo, H.; Sun, H.; Zhang, X.; Dai, X.; Luan, C.; Qin, C.; Zhao, H.; Li, J.; Wang, M.; Ye, J.-Y.; Sun, S.-G. Implanting Mo atoms into surface lattice of Pt_3Mn alloys enclosed by high-indexed facets: Promoting highly active sites for ethylene glycol oxidation. *ACS Catal.* **2018,** *9*, 442–455.
21. Meng, T.; Shang, N.; Zhao, J.; Su, M.; Wang, C.; Zhang, Y. Facile one-pot synthesis of Co coordination polymer spheres doped macroporous carbon and its application for electrocatalytic oxidation of glucose. *J. Colloid Interface Sci.* **2021,** *589*, 135–146.
22. Wang, G. Q.; Gu, J. F.; Zhuo, S. P. High dispersion Pt nanoparticles using mesoporous carbon support for enhancing conversion efficiency of dye-sensitized solar cells. *Chin. Chem. Lett.* **2010,** *21*, 1513–1516.
23. Xie, B.; Zhang, Y.; Du, N.; Li, H.; Hou, W.; Zhang, R. Preparation of preferentially exposed poison-resistant Pt(111) nanoplates with a nitrogen-doped graphene aerogel. *Chem. Commun.* **2016,** *52*, 13815–13818.
24. Beltrán-Gastélum, M.; Salazar-Gastélum, M. I.; Félix-Navarro, R. M.; Pérez-Sicairos, S.; Reynoso-Soto, E. A.; Lin, S. W.; Flores-Hernández, J. R.; Romero-Castanon, T.; Albarrán-Sánchez, I. L.; Paraguay-Delgado, F. Evaluation of Pt-Au/MWCNT (Multi-walled Carbon Nanotubes) electrocatalyst performance as cathode of a proton exchange membrane fuel cell. *Energy* **2016,** *109*, 446–455.
25. Liu, J.; Li, C.; Niu, H.; Wang, D.; Xin, C.; Liang, C. Low-energy hemiacetal dehydrogenation pathway: Co-production of gluconic acid and green hydrogen via glucose dehydrogenation. *Chem. - Asian J.* **2022,** *17*, 202200138.
26. Akiyama, S.; Nakagawa, K. Effect of mesopores in the Marimo nanocarbon anode material on the power generation performance of direct glucose fuel cell. *Carbon Trends* **2021,** *4*, 100058.
27. Sun, H.; Zeng, Q.; Ye, C.; Zhu, Y.; Chen, F.; Yang, M.; Fu, L.; Du, S.; Yu, J.; Jiang, N.; Liu, J.; Wu, T.; Lin, C.-T. Pt nanodendrites with (111) crystalline facet as an efficient, stable and pH-universal catalyst for electrochemical hydrogen production. *Chin. Chem. Lett.* **2020,** *31*, 2478–2482.
28. Zhou, Z. Y.; Huang, Z. Z.; Chen, D. J.; Wang, Q.; Tian, N.; Sun, S. G. High-index faceted platinum nanocrystals supported on carbon black as highly efficient catalysts for ethanol electrooxidation. *Angew. Chem. Int. Ed.* **2010,** *49*, 411–414.
29. Zhao, Y.; Fan, L.; Gao, D.; Ren, J.; Hong, B. High-power non-enzymatic glucose biofuel cells based on three-dimensional platinum nanoclusters immobilized on multiwalled carbon nanotubes. *Electrochim. Acta* **2014,** *145*, 159–169.
30. Zhang, X.; Zheng, J. High-index {hk0} facets platinum concave nanocubes loaded on multiwall carbon nanotubes and graphene oxide nanocomposite for highly sensitive simultaneous detection of dopamine and uric acid. *Talanta* **2020,** *207*, 120296.
31. Quan, Z.; Wang, Y.; Fang, J. High-index faceted noble metal nanocrystals. *Acc. Chem. Res.* **2013,** *46*, 191–202.
32. Ahmad, Y. H.; Mohamed, A. T.; El-Shafei, A.; Al-Qaradawi, S. Y.; Aljaber, A. S. Facile one-step synthesis of supportless porous AuPtPd nanocrystals as high performance electrocatalyst for glucose oxidation reaction. *Int. J. Hydrogen Energy* **2020,** *45*, 19163–19173.
33. Chetty, R.; Kundu, S.; Xia, W.; Bron, M.; Schuhmann, W.; Chirila, V.; Brandl, W.; Reinecke, T.; Muhler, M. PtRu nanoparticles supported on nitrogen-doped multiwalled carbon nanotubes as catalyst for methanol electrooxidation. *Electrochim. Acta* **2009,** *54*, 4208–4215.
34. Lee, S. R.; Park, J.; Gilroy, K. D.; Yang, X.; Figueroa-Cosme, L.; Ding, Y.; Xia, Y. Palladium@platinum concave nanocubes with enhanced catalytic activity toward oxygen reduction. *ChemCatChem* **2016,** *8*, 3082–3088.
35. Do, U. P.; Seland, F.; Wang, K.; Johannessen, E. A. Raney-platinum thin film electrodes for the catalysis of glucose in abiotically catalyzed micro-glucose fuel cells. *J. Mater. Sci.* **2019,** *54*, 14143–14156.
36. Łukaszewski, M.; Soszko, M.; Czerwiński, A. Electrochemical methods of real surface area determination of noble metal electrodes – an overview. *Int. J. Electrochem. Sci.* **2016,** *11*, 4442–4469.
37. Li, G.; Wang, Y.; Yu, F.; Lei, Y.; Hu, Z. Deep oxidization of glucose driven by 4-acetamido-TEMPO for a glucose fuel cell at room temperature. *Chem. Commun.* **2021,** *57*, 4051–4054.
38. Toghill, K. E.; Compton, R. G. Electrochemical non-enzymatic glucose sensors: A perspective and an evaluation. *Int. J. Electrochem. Sci.* **2010,** *5*, 1246–1301.
39. Beden, B.; Largeaud, F.; Kokoh, K. B.; Lamy, C. Fourier transform infrared reflectance spectroscopic investigation of the electrocatalytic oxidation of D-glucose: Identification of reactive intermediates and reaction products. *Electrochim. Acta* **1996,** *41*, 701–709.

 doi:10.20944/preprints202210.0183.v1

40. Torigoe, K.; Takahashi, M.; Tsuchiya, K.; Iwabata, K.; Ichihashi, T.; Sakaguchi, K.; Sugawara, F.; Abe, M. High-power abiotic direct glucose fuel cell using a gold–platinum bimetallic anode catalyst. *ACS Omega* **2018,** *3*, 18323−18333.
41. Burke, L. D. Premonolayer oxidation and its role in electrocatalysis. *Electrochim. Acta* **1994,** *39*, 1841−1848.
42. Tian, K.; Prestgard, M.; Tiwari, A. A review of recent advances in nonenzymatic glucose sensors. *Mater. Sci. Eng., C* **2014,** *41*, 100−118.
43. Xu, X.; Ma, Z.; Li, D.; Su, Z.; Dong, X.; Huang, H.; Qi, M. Pt concave nanocubes with high-index facets as electrocatalysts for glucose oxidation. *ACS Appl. Nano Mater.* **2022,** *5*, 4983−4990.
44. Chu, T.-F.; Lin, F.-Y.; Kuznetsova, I.; Wang, G.-J. A novel neutral non-enzymatic glucose biofuel cell based on a Pt/Au nano-alloy anode. *J. Power Sources* **2021,** *486*, 229374.